Thermochemistry and Kinetics of Hydrogen Abstraction by Methyl Radical from Polycyclic Aromatic Hydrocarbons

Karen Hemelsoet,*,†,‡ Veronique Van Speybroeck,† Damian Moran,‡,§ Guy B. Marin,|| Leo Radom,*,‡,§ and Michel Waroquier*,†

Center for Molecular Modeling, Proeftuinstraat 86, and Laboratorium voor Petrochemische Techniek, Krijgslaan 281-S5, Ghent University, B-9000 Ghent, Belgium, and School of Chemistry and ARC Centre of Excellence in Free Radical Chemistry and Biotechnology, University of Sydney, Sydney, NSW 2006, Australia

Received: August 9, 2006; In Final Form: October 12, 2006

Thermodynamic and kinetic properties relating to hydrogen abstraction by methyl radical from various sites in polycyclic aromatic hydrocarbons (PAHs) have been investigated. The reaction enthalpies (298 K), barriers (0 K), and activation energies and pre-exponential factors (700−1100 K), have been calculated by means of density functional theory, specifically with B3-LYP/6-311G(d,p) geometries, followed by BMK/6-311+G-(3df,2p) single-point energy calculations. For uncongested sites in the PAHs, a reasonable correlation is obtained between reactivities (as characterized by the reaction barriers) and reaction enthalpies. This is reflected in a Bell−Evans−Polanyi (BEP) relationship. However, for congested sites, abstraction is accompanied both by lower reaction enthalpies (due to relief of steric strain) and also by reduced reactivities (due to significantly increased steric hindrance effects in the transition structures), so that the BEP relationship does not hold. In addition, the reaction enthalpies and kinetic parameters for the series of linear acenes indicate that abstraction is more difficult from the central rings.

1. Introduction

Polycyclic aromatic hydrocarbons (PAHs) are widely studied organic molecules.[1,2] They play a key role in a large number of different areas as they are both naturally occurring and anthropogenic. PAHs are the largest known class of chemical carcinogens and mutagens.[3−5] They are present in atmospheric aerosols and many celestial objects such as meteorites, planetary nebulae, reflection nebulae, and active galaxies,[6−8] and recent work has reported spectroscopic evidence for the existence of PAHs in interstellar space.[9] Their importance in the formation process of hollow-cage fullerenes is also known.[10] In addition, PAHs are key intermediate products in soot formation and coal conversion processes.[11−14] They can arise as side products in steam cracking units used in the petrochemical industry for the production of light alkenes such as ethene and propene.[15] In this light, a quantitative understanding of the formation of PAH molecules is important for the efficient design of clean and practical combustion devices such as engines and incinerators and for a maximal run length of steam cracking units.

PAHs can grow by means of a radical reaction network. The model that begins with a phenyl radical, proposed by Frenklach et al.,[14] currently seems to be the most favored synthetic route. This model proposes a sequential addition of acetylene molecules to the phenyl radical to form mainly planar, naphthalene-like PAHs consisting of (substituted) six-membered rings. More recently, Vereecken et al.[16] have studied the growth of PAHs incorporating five-membered rings, which can also act as possible intermediates for the formation of nonplanar systems, including fullerenes. In the PAH growth processes, various classes of elementary reactions such as hydrogen abstraction, addition, cyclization, and dehydrogenation can be distinguished, and these lead to the formation of a surface consisting of conjugated rings.[16,17]

To model these potentially complex reaction processes, calculations on the contributing elementary reactions are desirable, as they provide the opportunity to obtain the required levels of insight and understanding for model genesis.[18−24] The initial step that allows formation of radical surface species involves hydrogen-abstraction reactions by means of gas-phase radicals, such as methyl and hydrogen.[24−27] In an earlier study,[27] we performed an elaborate level-of-theory investigation of hydrogen abstraction from benzene by methyl radical, as this reaction represents a fundamental point of comparison for radical-mediated hydrogen abstractions from the benzenoid components of PAHs. We found that virtually all the theoretical procedures that we examined were suitable for geometry optimization. However, for the reaction enthalpy, W1, G3-RAD, and UR-CCSD(T) yielded the best agreement with experiment. For the reaction barriers, URCCSD(T) and the low-cost BMK method provided values in close agreement with the benchmark value. Overall, G3-RAD, URCCSD(T), and the cost-effective density functional theory (DFT) methods BMK, BB1K, and MPW1K were found to give the best results for calculating the thermochemistry and kinetics of hydrogen abstraction by the methyl radical from benzene.

Some earlier studies have reported on the characteristics and reactivity of aryl radicals derived from PAHs, though theoretical studies have been complicated by the large spin contamination in the phenyl radical at the unrestricted Hartree−Fock level of theory.[28] On the basis of electron spin resonance studies and

* To whom correspondence should be addressed: e-mail karen.hemelsoet@UGent.be (K.H.), radom@chem.usyd.edu.au (L.R.), or michel.waroquier@UGent.be (M.W.).

† Center for Molecular Modeling, Ghent University.

‡ School of Chemistry, University of Sydney.

§ ARC Centre of Excellence in Free Radical Chemistry and Biotechnology, University of Sydney.

|| Laboratorium voor Petrochemische Techniek, Ghent University.

10.1021/jp065141n CCC: $33.50
Published on Web 11/30/2006

analysis of the spectra, in combination with theoretical calculations, Kasai et al.[29] showed that the aryl radicals that they investigated were all σ-radicals, with the unpaired electron found to occupy the essentially nonbonding σ-orbital corresponding to the broken bond. Also, by use of semiempirical calculations and by examining the bond dissociation energy (BDE), it was found that the strength of the aryl−H bond is essentially independent of molecular size but is more dependent on the environment around the C−H bond, and a classification into three types of aryl radicals was proposed.[30,31] Aihara et al.[32] used a PM3 approach in combination with a restricted open-shell Hartree−Fock (ROHF) procedure, and showed that the C−H BDE values were fairly constant for their test set. They reported that small variations in the calculated BDE values were primarily determined by the local structure near the abstraction site. This was supported by a good correlation between the BDE values and corresponding ∠CCC angles, calculated at the abstraction site of the reactant. DFT calculations performed by Cioslowski et al.[33] with the B-LYP functional indicated that there is a thermodynamic preference for the hydrogen in H-abstraction reactions to be preferentially removed from congested regions of the parent hydrocarbons, suggesting that the site specificity of the hydrogen abstraction is strongly influenced by steric factors. In a previous study,[34] we carefully investigated the bond dissociation enthalpies at 298 K for an extended set of hydrocarbons and corresponding ethynyl, aryl, vinyl, alkyl, propargyl, benzyl, and allyl radicals. In that study, the possible aryl radicals produced from PAHs were classified into six groups according to their C−H bond strengths.

The main goal of the present work is to obtain thermodynamic and kinetic data for hydrogen abstraction by methyl radical from a variety of possible sites in polycyclic aromatic hydrocarbons. The influence of the local environment on the C−H bond strengths of the PAHs and the thermodynamics and kinetics of the corresponding abstraction reactions will be emphasized. We compute optimized geometries, reaction enthalpies at 298 K (ΔH_{298}), barriers at 0 K ($\Delta E_0^{\ddagger}$), and activation energies (E_a), pre-exponential factors (A), and rate constants [$k(T)$] within a relevant temperature interval (700−1100 K). By studying the variations in the activation energy and pre-exponential factor in terms of the details of the polycyclic structure, we aim to gain insights as to which sites are preferred for the initial formation of surface radicals in a polycyclic aromatic network.

2. Theoretical Procedures

All calculations were performed with the Gaussian 03[35] software package. Geometries were optimized at the B3-LYP[36] level of theory, in conjunction with the 6-311G(d,p) basis set.[37] As mentioned earlier, a previous study on the reference hydrogen-abstraction reaction in benzene showed the limited influence of the level of theory on the optimized geometries.[27] Other studies on related radical reactions also reported that B3-LYP gives a reliable and quantitatively good description of geometries.[38,39] Frequencies were computed at the same level of theory as the geometry optimizations to provide zero-point vibrational energies (ZPVEs) and thermal corrections to the enthalpy and to confirm the nature of the stationary points. A scale factor of 0.9806 was used to obtain the ZPVEs from the calculated harmonic vibrational frequencies,[40] while unscaled frequencies were used to obtain the thermal corrections to the enthalpy. The use of scale factors provides a means of accounting for systematic deviations between measured and computed frequency-dependent properties and is an important consideration for the accurate description of reaction kinetics and thermochemistry.[40−42]

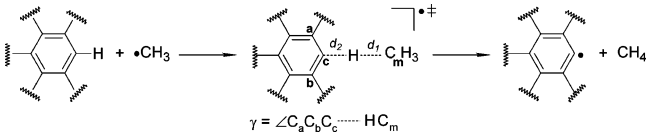

Figure 1. Hydrogen abstraction by the methyl radical from a model PAH to form an aryl radical plus methane. The forming bond length (d_1), breaking bond length (d_2), and out-of-plane angle (γ = angle between the $C_aC_bC_c$ plane and the H−CH_3 line) of the transition structure are highlighted.

Single-point energy calculations were performed by use of the BMK functional in conjunction with the 6-311+G(3df,2p) basis set. The BMK functional was recently developed by Boese and Martin[43] and is accurate to approximately 10 kJ mol^{-1} for the calculation of reaction barriers. The good performance of BMK appears to hinge on the combination of a high percentage of Hartree−Fock exchange (42%), together with terms dependent on the kinetic energy density, resulting in a "back-correction" for excessive HF exchange in systems where this would be undesirable. The BMK functional was also found to be a method of choice in our level-of-theory study on the abstraction reaction in benzene,[27] as it is an accurate computational method and yet affordable for systems of moderately large size, such as those studied in the present work.

We applied transition-state theory (TST),[44] including the incorporation of Eckart tunneling correction factors,[45] to calculate the rate constants $k(T)$. The Eckart method is a simple procedure that requires only a consideration of the stationary points on the reaction pathway and is therefore compatible with TST, although the method is often found to overestimate the tunneling contribution, especially at very low temperatures.[46] The link with the macroscopic quantities found in the Arrhenius rate law is made by a linear fit of ln $k(T)$ values, calculated for a range of temperatures, versus $1/T$. One refinement in our theoretical treatment comes from the observation that the transition structures (TSs) for the hydrogen-abstraction reactions have a very low frequency vibration, corresponding to internal rotation of the incoming methyl group about the forming bond. The standard harmonic oscillator (HO) model is known to be inappropriate for such modes and other approximations, such as the free rotor (FR)[19,47] or hindered rotor (HR)[48,49] model, are therefore used for this mode. The choice of a particular description depends on the height of the rotational barrier and the temperature. In a recent study of radical-addition reactions, we demonstrated the importance of correctly describing hindered internal rotations in order to obtain reliable partition functions.[19,50] In the present work, a mixed harmonic oscillator/free rotor (HO/FR) or mixed harmonic oscillator/hindered rotor (HO/HR) model, in which all the internal motions except for the methyl torsion in the TS are approximated as independent harmonic oscillators, was used.

3. Results and Discussion

Hydrogen abstraction by an approaching methyl radical from various sites in selected polycyclic aromatic hydrocarbons, leading to the formation of aryl radicals plus methane, have been studied. A schematic representation of the reactions that have been investigated is displayed in Figure 1, while the PAH molecules that have been studied, including our numbering scheme, are depicted in Figure 2. Our test set of PAHs can be divided into two subcategories. The first group includes the series of linear acenes, consisting of benzene (B), naphthalene (N), anthracene (A), tetracene (T), and pentacene (P). The other group consists of the nonlinear structures, including phenan-

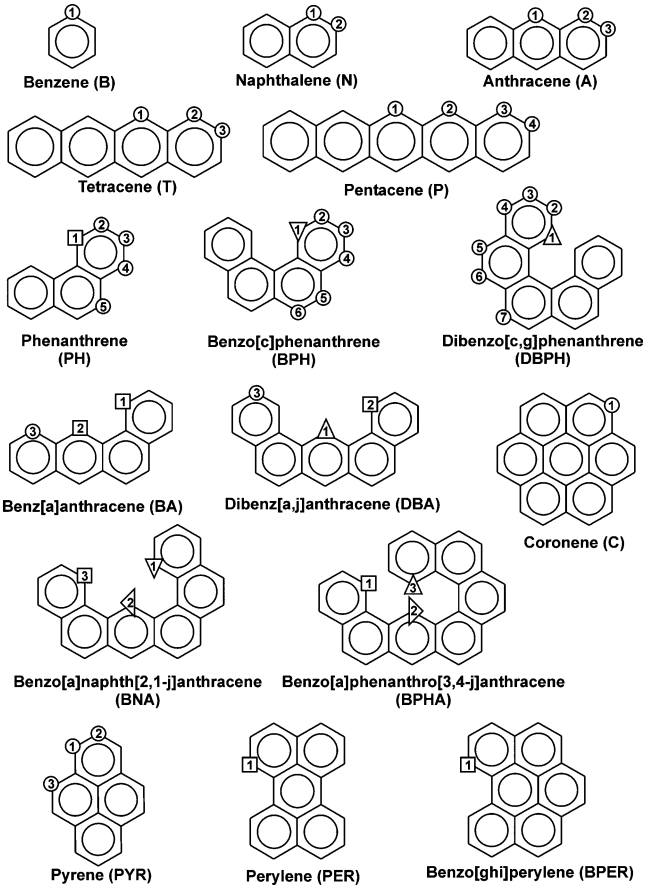

Figure 2. PAHs examined in the present study. Sites where hydrogen abstraction is considered are numbered. The sites are labeled on the basis of the hydrogen-abstraction enthalpy classifications (see text) (○ for B sites, □ for PH sites, ▽ for BPH sites, △ for DBPH sites, triangle pointing left for BNA sites, and triangle pointing right for BPHA sites).

threne (PH), benzo[*c*]phenanthrene (BPH), dibenzo[*c*,*g*]phenanthrene (DBPH), benz[*a*]anthracene (BA), dibenz[*a*,*j*]anthracene (DBA), coronene (C), benzo[*a*]naphth[2,1-*j*]anthracene (BNA), benzo[*a*]phenanthro[3,4-*j*]anthracene (BPHA), pyrene (PYR), perylene (PER), and benzo[*ghi*]perylene (BPER). The largest of these systems is coronene, which includes seven six-membered aromatic rings. Throughout this article, the notation PAH-X refers to the abstraction of hydrogen atom X from the polycyclic aromatic hydrocarbon PAH.

3.1. Geometries. The geometries of the PAHs, aryl radical products, and TSs were optimized at the B3-LYP/6-311G(d,p) level of theory. We note to begin that all the product radicals are of the σ-type, with the unpaired electron almost completely localized on a single carbon atom.[29] The corresponding spin densities of these product aryl radicals are given in Table S1 of the Supporting Information and clearly indicate the localization of the unpaired electron. Consequently, most geometrical perturbations resulting from the removal of a hydrogen atom are localized, systematic, and predictable.

A key geometrical feature is the planarity of most of the reactant PAHs and product aryl radicals. Four exceptions are found among the PAH molecules, specifically BPH, DBPH, BNA, and BPHA. Because of steric repulsive interactions between a pair of closely positioned hydrogen atoms, these molecules show significant deviations from planarity (Figure 3). In the first two structures, the deviations from planarity amount to approximately 18° within the phenanthrene component and 30° between the two phenanthrene components in DBPH. The BNA and BPHA structures can be regarded as

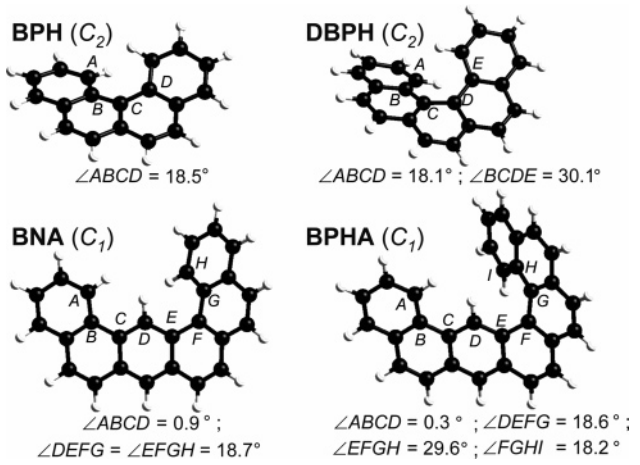

Figure 3. B3-LYP/6-311G(d,p) optimized geometries of nonplanar PAHs BPH, DBPH, BNA, and BPHA, including dihedral angles that measure the degree of nonplanarity.

combinations of two smaller PAH structures, specifically PH and BPH in the case of BNA and PH and DBPH in the case of BPHA. The deviations from planarity are mainly confined to the BPH and DBPH moieties, respectively, and similar dihedral angles of approximately 18° and 30° are found in these substructures. The nonplanarity is to a large extent removed when the aryl radicals BPH-1, BNA-1, and BNA-2 (see Figure 2) are formed, following the abstraction of a hydrogen atom. In the case of the DBPH-1, BPHA-2, and BPHA-3 radicals, the deviations from planarity for the twisted plane where the hydrogen is abstracted are significantly reduced. This is reflected in dihedral angles of 7.6°, 10.2°, and 6.5°, respectively, for $\angle ABCD$, $\angle DEFG$, and $\angle FGHI$ (as defined in Figure 3) of the corresponding aryl radicals. Other important geometrical features in the PAHs and the product radicals are the changes in bond distances and angles at the hydrogen-abstraction site. The perturbations associated with removal of a hydrogen atom lead to shortening of the adjacent C−C bonds by approximately 0.02 Å, as well as widening of the bond angle at the carbon from which abstraction has taken place by about 6°. Similar results were noted previously by Cioslowski et al.[33] for a test set of 10 PAHs containing up to five six-membered rings.

For the transition structures for hydrogen abstraction, the forming (d_1) and breaking (d_2) bond lengths, as well as the out-of-plane angle (γ) of the approaching methyl radical, are the salient geometrical features. These parameters are illustrated in Figure 1, and the computed results are included in Table 1. It can be seen that, for most structures, d_1 is modestly shorter than d_2 (average difference approximately 0.07 Å), which is consistent with a "late" (in the Hammond sense) TS and in accordance with the reaction endothermicity. Exceptions are found for DBA-1, BNA-2, and BPHA-2, where the d_2 bond length is slightly shorter than the d_1 bond length (average difference approximately 0.02 Å). This behavior can be traced back to the more folded structures for the TSs in these cases, as illustrated in Figure 4. It can also be seen that for the abstraction of hydrogen atoms located at some of the more congested sites of the PAHs, the approaching methyl radical is forced to follow an out-of-plane pathway. For these TSs, the out-of-plane angle γ ranges from 11.9° (for PER-1) to 40.8° (for BNA-2). These large values of γ are basically due to steric hindrance between the incoming methyl radical and the closely positioned hydrogen atoms.

3.2. Reaction Enthalpies and Barriers. ΔH_{298} and $\Delta E_0^{\ddagger}$ values for the reactions between the various PAHs and the

TABLE 1: Forming (d_1) and Breaking (d_2) Bond Lengths and Out-of-Plane Angles γ in the Transition Structures for Hydrogen Abstraction from PAHs by Methyl Radical[a]

site	d_1 (Å)	d_2 (Å)	γ (deg)	site	d_1 (Å)	d_2 (Å)	γ (deg)
TS:B-1	1.307	1.379	0.1	TS:DBPH-1	1.322	1.362	21.6
TS:N-1	1.308	1.381	0.0	TS:DBPH-2	1.305	1.379	0.8
TS:N-2	1.305	1.380	0.0	TS:DBPH-3	1.304	1.381	2.4
TS:A-1	1.313	1.385	0.0	TS:DBPH-4	1.309	1.380	2.5
TS:A-2	1.308	1.381	0.0	TS:DBPH-5	1.306	1.383	4.5
TS:A-3	1.306	1.379	0.0	TS:DBPH-6	1.308	1.380	1.1
TS:T-1	1.312	1.385	0.3	TS:DBPH-7	1.306	1.383	3.9
TS:T-2	1.308	1.380	0.0	TS:BA-1	1.322	1.373	0.1
TS:T-3	1.306	1.379	0.0	TS:BA-2	1.333	1.368	22.6
TS:P-1	1.314	1.382	0.0	TS:BA-3	1.308	1.381	0.6
TS:P-2	1.313	1.383	0.0	TS:DBA-1	1.355	1.343	38.9
TS:P-3	1.308	1.380	0.0	TS:DBA-2	1.323	1.371	0.1
TS:P-4	1.306	1.379	0.0	TS:DBA-3	1.305	1.380	0.1
TS:PH-1	1.323	1.373	0.2	TS:BNA-1	1.332	1.354	26.9
TS:PH-2	1.305	1.380	0.0	TS:BNA-2	1.361	1.331	40.8
TS:PH-3	1.304	1.382	0.0	TS:BNA-3	1.322	1.371	17.2
TS:PH-4	1.308	1.382	0.0	TS:BPHA-1	1.318	1.373	14.1
TS:PH-5	1.308	1.381	0.0	TS:BPHA-2	1.355	1.338	37.5
TS:BPH-1	1.333	1.352	26.0	TS:BPHA-3	1.323	1.361	22.2
TS:BPH-2	1.306	1.378	2.5	TS:C-1	1.307	1.382	0.0
TS:BPH-3	1.303	1.382	2.6	TS:PYR-1	1.305	1.384	0.0
TS:BPH-4	1.309	1.380	1.8	TS:PYR-2	1.305	1.380	0.0
TS:BPH-5	1.306	1.383	3.2	TS:PYR-3	1.308	1.381	0.0
TS:BPH-6	1.308	1.381	2.2	TS:PER-1	1.322	1.370	11.9
				TS:BPER-1	1.321	1.374	0.0

[a] See Figure 1 for definitions of d_1, d_2, and γ. Transition structures were optimized at the B3-LYP/6-311G(d,p) level.

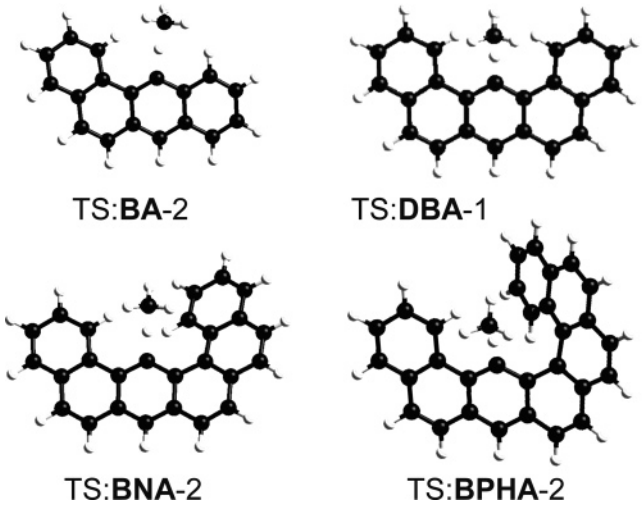

Figure 4. B3-LYP/6-311G(d,p) optimized geometries of the transition structures for hydrogen abstraction by methyl radical at congested sites.

methyl radical were calculated at the BMK/6-311+G(3df,2p)//B3-LYP/6-311G(d,p) level, by use of scaled ZPVEs and thermal corrections.[51] The results are given in Table 2.

3.2.1. Reaction Enthalpies. Inspection of the results in Table 2 shows that the hydrogen-abstraction enthalpies lie within a broad range between −1.8 (BNA-2) and +34.3 (A-1, T-1) kJ mol^{-1}. The reactions are endothermic with the exception of the BNA-2 reaction, which is slightly exothermic. A clustering of the reaction enthalpies into six groups is observed, as illustrated in Figure S1 of the Supporting Information. This had previously been noted, on the basis of BDE values.[34] Averages of the computed ΔH_{298} values for each of these groups X ($\langle \Delta H_{298} \rangle_X$) can be determined. In order of decreasing reaction enthalpies, we distinguish B-like sites ($\langle \Delta H_{298} \rangle_B$ = 32.0 kJ mol^{-1}), PH-like sites ($\langle \Delta H_{298} \rangle_{PH}$ = 25.0 kJ mol^{-1}), DBPH-like sites ($\langle \Delta H_{298} \rangle_{DBPH}$ = 18.4 kJ mol^{-1}), BPHA-like sites ($\langle \Delta H_{298} \rangle_{BPHA}$ = 12.1 kJ mol^{-1}), BPH-like sites ($\langle \Delta H_{298} \rangle_{BPH}$ = 4.5 kJ mol^{-1}), and BNA-like sites ($\langle \Delta H_{298} \rangle_{BNA}$ = −1.8 kJ mol^{-1}). Figure 2 shows the hydrogen atoms that belong to the various categories.

In earlier work, classifications based on other properties have been proposed. For example, in one study involving a smaller test set of six PAHs (B, N, A, PH, BPH, and DBPH),[24] the various abstraction sites were differentiated on the basis of a qualitative description of the local environment of the sites, specifically the number of intermediate carbon atoms between the hydrogen to be abstracted and the closest adjacent hydrogen atom. There is significant overlap between this classification and that based on reaction enthalpies, indicating the important role of the local environment of the hydrogen-abstraction site on the C−H bond strength. We note, however, that sometimes these clusters of values are coincidental rather than intrinsic. For example, the ΔH_{298} value for the DBPH-1 site amounts to 19.3 kJ mol^{-1}, which is close to the 19.0 kJ mol^{-1} for DBA-1, despite the local environments for the DBPH-1 and DBA-1 sites clearly being quite different.

Detailed analysis of the series of linear acenes reveals that the various sites (previously all classified as B-like sites) can be subdivided into three categories. The first group corresponds to hydrogen atoms located in the outer rings of the linear acenes, and the nomenclature B-like sites remains appropriate for this type. An average value of $\langle \Delta H_{298} \rangle_B$ = 30.5 kJ mol^{-1} is obtained. The second and third groups correspond to naphthalene- (N-) and anthracene- (A-) like sites, with $\langle \Delta H_{298} \rangle_N$ = 31.8 kJ mol^{-1} and $\langle \Delta H_{298} \rangle_A$ = 34.1 kJ mol^{-1}, respectively. The latter group of A-type hydrogens are sometimes referred to as solo hydrogens,[32] that is, hydrogen atoms bonded to sp^2-carbon atoms with no adjacent C−H bonds. In agreement with the study of Aihara et al.,[32] the calculated enthalpy values corresponding to these solo atoms are found to be the largest in the particular PAH molecule being considered.

It is concluded overall that the reaction enthalpies for abstraction at the more congested sites correspond to smaller (less positive or more negative) enthalpy values, due to a relief from steric hindrance upon creation of the radical, in accordance with previous conclusions of Cioslowski et al.[52]

3.2.2. Reaction Barriers. The calculated hydrogen-abstraction barriers at 0 K ($\Delta E_0^{\ddagger}$) are included in Table 2. The barriers are relatively high, lying between 70.8 (P-4) and 89.2 (DBA-1) kJ mol^{-1}. It can be seen that the steric hindrance effects the methyl radical encounters when approaching the abstraction site become very important for the more congested sites. In such circumstances, they contribute to a significant increase in the reaction barrier with respect to the barrier of 71.8 kJ mol^{-1} for the abstraction in benzene. The most striking examples of increased barriers are seen for the abstractions at DBA-1, BA-2, BNA-2, and BPHA-2, with barriers amounting to 89.2, 82.9, 80.7, and 82.2 kJ mol^{-1}, respectively. The optimized geometries of the corresponding TSs (Figure 4) reveal high values for the out-of-plane angles (explicitly given in Table 1, e.g., 38.9° for DBA-1), which is a reflection of the steric hindrance encountered by the methyl radical.

Inspection of the results in Table 2 does not show any general correlation between the ΔH_{298} and $\Delta E_0^{\ddagger}$ results. Indeed, a scatter plot is obtained when these quantities are plotted against one another (Figure 5a). We observe that greater congestion generally leads to reduced reactivity for hydrogen abstraction by a methyl radical (because the site becomes less accessible), in contrast to the greater reactivity that would have been anticipated to accompany the lower reaction enthalpies (relief of steric strain) with a normal (Bell−Evans−Polanyi) reactivity−enthalpy relationship.[53] On the other hand, for the series of linear

TABLE 2: Calculated Reaction Enthalpies and Barriers for Hydrogen Abstraction from Various Sites of the PAHs Shown in Figure 2[a]

site	B-1	N-1	N-2	A-1	A-2	A-3	T-1
ΔH_{298} (kJ mol^{-1})	30.6	32.1	30.8	34.3	31.9	30.8	34.3
$\Delta E_0^{\ddagger}$ (kJ mol^{-1})	71.8	72.7	71.7	74.8	72.6	71.3	74.6
site	T-2	T-3	P-1	P-2	P-3	P-4	PH-1
ΔH_{298} (kJ mol^{-1})	31.6	30.4	34.0	33.8	31.5	29.9	24.7
$\Delta E_0^{\ddagger}$ (kJ mol^{-1})	72.1	71.0	74.4	74.2	71.5	70.8	76.5
site	PH-2	PH-3	PH-4	PH-5	BPH-1	BPH-2	BPH-3
ΔH_{298} (kJ mol^{-1})	31.1	32.2	32.1	31.7	4.9	30.2	32.1
$\Delta E_0^{\ddagger}$ (kJ mol^{-1})	71.5	72.0	72.4	72.2	75.2	71.6	72.2
site	BPH-4	BPH-5	BPH-6	DBPH-1	DBPH-2	DBPH-3	DBPH-4
ΔH_{298} (kJ mol^{-1})	31.6	32.7	32.0	19.3	31.0	32.0	31.9
$\Delta E_0^{\ddagger}$ (kJ mol^{-1})	72.8	73.1	72.6	74.1	71.9	73.0	73.3
site	DBPH-5	DBPH-6	DBPH-7	BA-1	BA-2	BA-3	DBA-1
ΔH_{298} (kJ mol^{-1})	33.0	31.8	33.1	24.5	26.8	32.2	19.0
$\Delta E_0^{\ddagger}$ (kJ mol^{-1})	73.7	72.5	73.8	76.9	82.9	72.8	89.2
site	DBA-2	DBA-3	C-1	BNA-1	BNA-2	BNA-3	BPHA-1
ΔH_{298} (kJ mol^{-1})	23.6	31.2	34.0	4.0	-1.8	24.5	26.0
$\Delta E_0^{\ddagger}$ (kJ mol^{-1})	76.2	71.3	73.2	72.8	80.7	76.6	77.6
site	BPHA-2	BPHA-3	PYR-1	PYR-2	PYR-3	PER-1	BPER-1
ΔH_{298} (kJ mol^{-1})	12.1	16.9	33.7	30.8	31.8	23.7	25.9
$\Delta E_0^{\ddagger}$ (kJ mol^{-1})	82.2	73.5	73.3	71.5	71.9	77.0	76.8

[a] Energies were obtained at the BMK/6-311+G(3df,2p)//B3-LYP/6-311G(d,p) level.

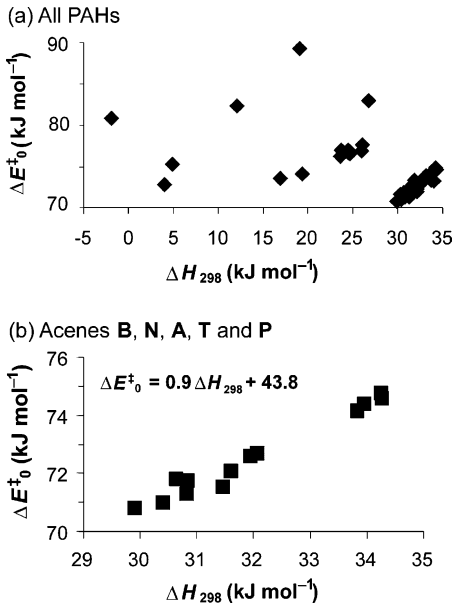

Figure 5. Barriers at 0 K ($\Delta E_0^{\ddagger}$) versus reaction enthalpies at 298 K (ΔH_{298}) for hydrogen-abstraction reactions at various sites of (a) all the PAHs examined and (b) only the series of linear acenes [BMK/6-311+G(3df,2p)//B3-LYP/6-311G(d,p)].

acenes, the Bell−Evans−Polanyi relationship does hold reasonably well, as illustrated in Figure 5b. For these uncongested regions, the approaching methyl radical does not encounter increased steric hindrance effects, and consequently a direct link between the strength of the C−H bond (as characterized by the ΔH_{298} values) and the reactivity toward abstraction (as characterized by the $\Delta E_0^{\ddagger}$ values) is expected and observed.

3.3. Kinetic Parameters and Rate Constants. Rate constants $k(T)$, and corresponding activation energies E_a and pre-exponential factors A, for the reactions between the various PAHs and methyl radical were calculated at the BMK/6-311+G(3df,2p)//B3-LYP/6-311G(d,p) level in the temperature interval of 700−1100 K, which is relevant for the steam cracking and coke formation processes. Two refinements are taken into consideration in the calculations: the effect of tunneling corrections on the one hand, and a refined description of the low-energy torsion of the methyl group in the TSs on the other. Details of the computed kinetic parameters can be found in Table S3 of the Supporting Information.

We find that the Eckart tunneling correction contributes an average downward shift of 4.5 kJ mol^{-1} to the activation energy, whereas it has only a modest effect on the pre-exponential factor, indicated by an average decrease by a factor of 1.3 in the ratio $A_{\text{with out tunneling}}/A_{\text{with tunneling}}$.

In order to establish a more detailed description of the low-lying vibrational mode corresponding to the internal rotation of the methyl group about the forming/breaking bond in the TSs, rotational potentials were computed. For the uncongested sites, the barrier height for the rotational potential was found to be very small, more precisely 0.1 kJ mol^{-1} or less, and the values of the methyl torsional frequency ν_m lie between 4.2 and 65.4 cm^{-1}. On this basis, the free rotor model was deemed appropriate to describe the methyl torsion, and a mixed harmonic oscillator/free rotor (HO/FR) model was used for the calculation of kinetic properties. For the congested sites (PH-, BPH-, DBPH-, BNA-, and BPHA-like sites), the methyl torsional barriers were found to be higher, with a maximum value of approximately 5 kJ mol^{-1} being obtained for DBA-1. The abstraction reactions at these sites show a larger value for the torsional frequency, a maximum value of 147.3 cm^{-1} being found for the abstraction at DBA-1. A one-dimensional hindered rotor model was chosen to model the internal rotation in these cases, and a mixed harmonic oscillator/hindered rotor (HO/HR) model was used for the calculation of kinetic properties. The influence of the refined treatment of internal rotations for the investigated hydrogen-abstraction reactions is not negligible. The activation energy is lowered by an average of 3.3 kJ mol^{-1}, while the pre-exponential factor decreases by a factor of 5.6 ($= A_{HO}/A_{mixed}$). The overall influence on the rate constant $k(T)$ amounts to average factors ($= k_{mixed}/k_{HO}$) of 0.59, 0.54, and 0.49 at 700, 900, and 1100 K, respectively.

3.3.1. Linear Acenes. For the series of linear acenes, we subdivided the abstraction sites as B, N, or A, all of which are uncongested locations where steric hindrance effects between the methyl radical and the PAH molecule are not important. The mixed HO/FR model was therefore used for the computa-

TABLE 3: Calculated Rate Constants, Activation Energies, and Pre-exponential Factors for Hydrogen Abstraction by Methyl Radical at Various Sites in Linear Acenes[a]

site	k_{700} (m^3 mol^{-1} s^{-1})	k_{900} (m^3 mol^{-1} s^{-1})	k_{1100} (m^3 mol^{-1} s^{-1})	E_a (kJ mol^{-1})	A (m^3 mol^{-1} s^{-1})
B-1	2.55×10^1	5.12×10^2	3.97×10^3	80.9	2.62×10^7
N-1	1.45×10^1	2.99×10^2	2.36×10^3	81.6	1.69×10^7
N-2	1.74×10^1	3.53×10^2	2.76×10^3	81.1	1.86×10^7
A-1	7.36×10^0	1.64×10^2	1.35×10^3	83.6	1.20×10^7
A-2	1.34×10^1	2.76×10^2	2.18×10^3	81.6	1.55×10^7
A-3	1.99×10^1	3.96×10^2	3.05×10^3	80.7	1.96×10^7
T-1	7.62×10^0	1.68×10^2	1.39×10^3	83.4	1.20×10^7
T-2	1.78×10^1	3.62×10^2	2.83×10^3	81.2	1.94×10^7
T-3	2.15×10^1	4.25×10^2	3.26×10^3	80.4	2.04×10^7
P-1	7.73×10^0	1.70×10^2	1.40×10^3	83.4	1.21×10^7
P-2	8.02×10^0	1.75×10^2	1.43×10^3	83.0	1.19×10^7
P-3	1.71×10^1	3.41×10^2	2.64×10^3	80.8	1.71×10^7
P-4	2.19×10^1	4.29×10^2	3.27×10^3	80.3	2.02×10^7

[a] Calculated by use of the mixed HO/FR model and including Eckart tunneling corrections. Energies were obtained at the BMK/6-311+G(3df,2p)//B3-LYP/6-311G(d,p) level.

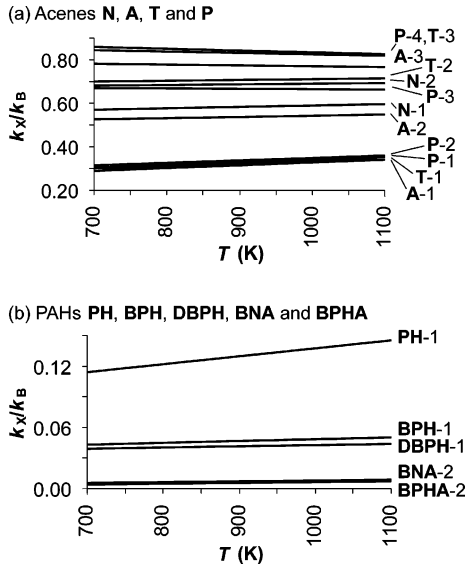

Figure 6. Ratios of calculated rate constants $k_X(T)/k_B(T)$ for hydrogen-abstraction reactions at the possible sites of (a) linear acenes and (b) nonlinear PAHs, within the temperature range 700−1100 K [BMK/6-311+G(3df,2p)//B3-LYP/6-311G(d,p) with HO/FR or HO/HR frequency models and including Eckart tunneling corrections; see text].

tion of the rate constants $k(T)$ in these cases. In Figure 6a, the rate constants for the hydrogen abstractions at N, A, T, and P are depicted, with the abstraction in benzene serving as a reference. Table 3 gives the rate constants at 700, 900, and 1100 K, together with the derived kinetic parameters. Abstraction from the benzene molecule is the fastest. Abstractions of a hydrogen atom located at a central ring, corresponding to A-like sites, or more precisely A-1, T-1, P-1, and P-2, are the slowest, approximately 3 times slower than abstraction in benzene. Abstraction reactions at noncentral rings (corresponding to B- and N-like sites) are preferred over abstraction at the central rings. This trend is supported by both kinetic parameters: the average activation energy is approximately 3 kJ mol^{-1} lower, while the pre-exponential factor is 1.7 times higher.

Another interesting aspect is the convergent behavior of the kinetic parameters and rate constants with increasing PAH size. Comparison of the kinetic parameters E_a and A for the abstraction reactions at B-1, N-1, A-1, T-1, and P-1 shows that limiting values are already reached for both parameters in the anthracene molecule, and this is also seen in Figure 6a. It thus appears sufficient to take into account three six-membered rings in order to adequately model the kinetics of the linear acenes.

3.3.2. Nonlinear PAHs. Calculated rate constants for a range of temperatures, as well as the associated kinetic parameters E_a and A, are given in Table 4 for the abstraction reactions for the nonlinear PAHs. Figure 6b depicts the ratio of the rate constant at the characteristic sites X with respect to the rate constant in benzene in the relevant temperature range. Inspection of the results obtained for the different categories PH-1, BPH-1, DBPH-1, BNA-2, and BPHA-2 reveals that the calculated $k(T)$ values for the less congested PAH molecules, for example, phenanthrene, are higher than those for the congested sites at all temperatures. Further examination of the results obtained for the abstraction at these (congested) non-B-like sites shows that the variation in the kinetic parameters is larger than in the series of linear acenes. The E_a values lie in the range 80.9−96.7 kJ mol^{-1}, while the A values vary between 5.3×10^5 and 1.0×10^7 m^3 mol^{-1} s^{-1}. The kinetic parameters corresponding to the six different categories based on reaction enthalpies are depicted in Figure 7. The pre-exponential factors clearly support the conclusion that the abstraction becomes more difficult as the PAH abstraction site becomes more congested. In addition, the E_a values for the very congested sites BNA-2 and BPHA-2 are substantially higher.

Detailed inspection of the results in Table 4 also shows that, even within a specific PAH, abstraction at B-like sites is always preferred over abstraction at more congested sites. For instance, for the various sites within the phenanthrene (PH) molecule, it can be seen that abstraction at the PH-like site (PH-1) is more difficult than abstractions at the B-like sites (PH-i, $i = 2-5$), as reflected in an average factor of 2.3 between the specific rate constants.

As a final remark, we note that comparison of the PH-1 and BPER-1 results offers valuable information about the possible consequences of adding an extra layer to the coke surface model. The deviations between the rate parameters for the two abstraction reactions are seen to be small, with a factor of approximately 1.6 being obtained for k(BPER-1)/k(PH-1) and small changes also being observed for the activation energy and pre-exponential factor.

4. Conclusion

In this study, hydrogen abstraction by an approaching methyl radical from a variety of sites in polycyclic aromatic hydrocarbons (PAHs) has been investigated by means of density functional theory calculations. Large systems, containing up to seven six-membered rings, have been examined, and the influence of the polycyclic environment on thermodynamic and kinetic properties has been explored. Optimized B3-LYP/6-

TABLE 4: Calculated Rate Constants, Activation Energies, and Pre-exponential Factors for Hydrogen Abstraction by Methyl Radical at Various Sites in Nonlinear PAHs[a]

site	k_{700} (m^3 mol^{-1} s^{-1})	k_{900} (m^3 mol^{-1} s^{-1})	k_{1100} (m^3 mol^{-1} s^{-1})	E_a (kJ mol^{-1})	A (m^3 mol^{-1} s^{-1})
PH-1	2.91×10^{0}	6.76×10^{1}	5.78×10^{2}	84.8	5.85×10^{6}
PH-2	8.62×10^{0}	1.73×10^{2}	1.34×10^{3}	80.8	8.78×10^{6}
PH-3	8.43×10^{0}	1.72×10^{2}	1.35×10^{3}	81.3	9.27×10^{6}
PH-4	6.39×10^{0}	1.30×10^{2}	1.01×10^{3}	81.2	6.89×10^{6}
PH-5	7.87×10^{0}	1.59×10^{2}	1.24×10^{3}	81.1	8.32×10^{6}
BPH-1	1.10×10^{0}	2.41×10^{1}	1.99×10^{2}	83.3	1.71×10^{6}
BPH-2	4.63×10^{0}	9.30×10^{1}	7.21×10^{2}	80.9	4.74×10^{6}
BPH-3	4.20×10^{0}	8.68×10^{1}	6.85×10^{2}	81.6	4.90×10^{6}
BPH-4	3.30×10^{0}	6.81×10^{1}	5.38×10^{2}	81.6	3.84×10^{6}
BPH-5	3.29×10^{0}	6.92×10^{1}	5.54×10^{2}	82.2	4.20×10^{6}
BPH-6	3.77×10^{0}	7.77×10^{1}	6.13×10^{2}	81.6	4.38×10^{6}
DBPH-1	9.96×10^{-1}	2.14×10^{1}	1.74×10^{2}	82.8	1.41×10^{6}
DBPH-2	4.31×10^{0}	8.77×10^{1}	6.87×10^{2}	81.3	4.72×10^{6}
DBPH-3	3.48×10^{0}	7.40×10^{1}	5.96×10^{2}	82.4	4.64×10^{6}
DBPH-4	2.79×10^{0}	5.86×10^{1}	4.69×10^{2}	82.1	3.54×10^{6}
DBPH-5	2.78×10^{0}	5.97×10^{1}	4.84×10^{2}	82.7	3.88×10^{6}
DBPH-6	3.37×10^{0}	6.92×10^{1}	5.44×10^{2}	81.5	3.81×10^{6}
DBPH-7	2.72×10^{0}	5.90×10^{1}	4.80×10^{2}	82.9	3.93×10^{6}
BA-1	1.92×10^{0}	4.61×10^{1}	4.02×10^{2}	85.6	4.44×10^{6}
BA-2	1.51×10^{-1}	4.53×10^{0}	4.57×10^{1}	91.6	9.71×10^{5}
BA-3	3.69×10^{0}	7.68×10^{1}	6.10×10^{2}	81.9	4.48×10^{6}
DBA-1	4.84×10^{-2}	1.76×10^{0}	2.02×10^{1}	96.7	7.44×10^{5}
DBA-2	3.79×10^{0}	8.65×10^{1}	7.32×10^{2}	84.4	7.03×10^{6}
DBA-3	9.51×10^{0}	1.90×10^{2}	1.47×10^{3}	80.8	9.54×10^{6}
BNA-1	1.19×10^{0}	2.38×10^{1}	1.86×10^{2}	80.9	1.23×10^{6}
BNA-2	1.42×10^{-1}	3.77×10^{0}	3.53×10^{1}	88.4	5.30×10^{5}
BNA-3	5.43×10^{-1}	1.27×10^{1}	1.09×10^{2}	84.9	1.11×10^{6}
BPHA-1	4.59×10^{-1}	1.12×10^{1}	9.83×10^{1}	86.0	1.13×10^{6}
BPHA-2	1.09×10^{-1}	3.09×10^{0}	3.00×10^{1}	90.0	5.33×10^{5}
BPHA-3	1.30×10^{0}	2.72×10^{1}	2.18×10^{2}	82.1	1.64×10^{6}
C-1	3.63×10^{1}	7.70×10^{2}	6.18×10^{3}	82.3	4.77×10^{7}
PYR-1	1.25×10^{1}	2.66×10^{2}	2.15×10^{3}	82.5	1.68×10^{7}
PYR-2	1.84×10^{1}	3.71×10^{2}	2.89×10^{3}	81.0	1.92×10^{7}
PYR-3	1.68×10^{1}	3.37×10^{2}	2.61×10^{3}	80.8	1.71×10^{7}
PER-1	2.24×10^{0}	5.31×10^{1}	4.60×10^{2}	85.3	4.93×10^{6}
BPER-1	4.71×10^{0}	1.11×10^{2}	9.59×10^{2}	85.2	1.01×10^{7}

[a] Calculated by use of the mixed HO/FR or HO/HR model and including Eckart tunneling corrections. Energies were obtained at the BMK/6-311+G(3df,2p)//B3-LYP/6-311G(d,p) level.

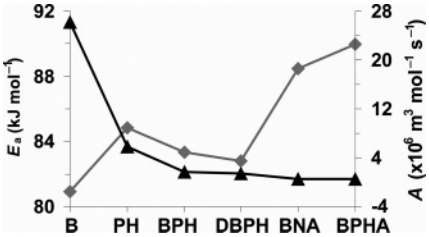

Figure 7. Average values of activation energies (◆, E_a, kJ mol^{-1}) and pre-exponential factors (▲, A, m^3 mol^{-1} s^{-1}) for PAH groups [BMK/6-311+G(3df,2p)//B3-LYP/6-311G(d,p) with HO/FR or HO/HR frequency models and including Eckart tunneling corrections; see text].

311G(d,p) geometries and subsequent BMK/6-311+G(3df,2p) single-point energy calculations have been used, leading to the following conclusions.

The congested sites in the PAHs correspond to lower reaction enthalpy values, largely reflecting the release of steric strain upon creation of the radical. The reaction barriers on the other hand show that abstraction at these congested locations is more difficult, as the site becomes less accessible for the approaching methyl radical. Consequently, a Bell−Evans−Polanyi relationship is not obtained. However, analysis of the subset of linear acenes does indicate a good correlation between reactivities and reaction enthalpies, since in this case we are dealing with uncongested locations and steric hindrance effects in the TSs are not important.

Rate constants, activation energies, and pre-exponential factors, calculated in the temperature interval 700−1100 K, support the observation that abstraction at the uncongested benzene-like sites is preferred for the initial formation of radical species. For the series of linear acenes, the kinetic parameters are found to vary modestly, whereas for the expanded test set, larger variations are observed. For calculation of the rate constants, two refinements are taken into account, specifically Eckart tunneling corrections and an improved description of the internal rotation of the incoming methyl group about the breaking/forming bond in the transition structure. The latter effect reduces the rate constant by a factor of about 1.9 (at a temperature of 900 K). The tunneling corrections contribute to a shift in the activation energies by approximately 4.5 kJ mol^{-1}. Overall, the combination of both effects results in an average downward shift of 7.8 kJ mol^{-1} for the activation energies and a reduction by a factor of approximately 7.4 for the pre-exponential factors, leading to a decrease in the rate constants by a factor of 2.6.

Acknowledgment. K.H. thanks L.R. and members of his research group for their kind hospitality during her stay at the University of Sydney, where this work originated. D.M. thanks the University of Sydney for a Sesqui Postdoctoral Fellowship. V.V.S., G.B.M., and M.W. thank the Fund for Scientific Research−Flanders, and the Research Board of Ghent University. L.R. thanks the Australian Research Council for a Discovery Grant and the ARC Centre of Excellence in Free

Radical Chemistry and Biotechnology for funding and gratefully acknowledges generous allocations of computing time from the Australian Partnership for Advanced Computing, the Australian National University Supercomputing Facility, and the Australian Centre for Advanced Computing and Communication. Finally, we thank Professor Jan Martin for making the BMK functional available for our use.

Supporting Information Available: Reaction enthalpies at 298 K (Figure S1), structures of the PAHs that have been examined (Figure S2), spin densities of all product radicals (Table S1), total energies, zero-point vibrational energies, and thermal corrections (Table S2), and effect on activation energies and pre-exponential factors of the model used to provide a refined description of the low-energy torsional motion of the methyl group in the transition structures and effect of Eckart tunneling corrections (Table S3). This material is available free of charge via the Internet at http://pubs.acs.org.

References and Notes

(1) Gonzales, J. M.; Barden, C. J.; Brown, S. T.; Schleyer, P. v. R.; Schaefer, H. F., III; Li, Q.-S. *J. Am. Chem. Soc.* **2003**, *125*, 1064 and references therein.

(2) Watson, M. D.; Fechtenkötter, A.; Müllen, K. *Chem. Rev.* **2001**, *101*, 1267.

(3) (a) Harvey, R. G. *Polycyclic Aromatic Hydrocarbons: Chemistry and Carcinogenicity*; Cambridge University Press: Cambridge, U.K., 1991. (b) Harvey, R. G. *Polycyclic Aromatic Hydrocarbons*; Wiley−VCH: New York, 1997.

(4) Durant, J. L.; Busby, W. F.; Lafleur, A. L.; Penman, B. W.; Crespi, C. L. *Mutat. Res.* **1996**, *371*, 123.

(5) Denissenko, M. F.; Pao, A.; Tang, M. S.; Pfeifer, G. P. *Science* **1996**, *274*, 430.

(6) Allamandola, L. J. *Top Curr. Chem.* **1990**, *153*, 1.

(7) (a) *Polycyclic Aromatic Hydrocarbons and Astrophysics*; Léger, A., d'Hendecourt, L., Boccara, N., Eds.; NATO ASI Series C; Reidel: Dordrecht, The Netherlands, 1987; Vol. 191. (b) Puget, J. L.; Léger, A. *Annu. Rev. Astron. Astrophys.* **1989**, *27*, 161.

(8) Allen, J. O.; Dookeran, M.; Smith, K. A.; Sarofim, A. F.; Taghizadeh, K.; Lafleur, A. L. *Environ. Sci. Technol.* **1996**, *30*, 1023.

(9) Lovas, F. J.; McMahon, R. J.; Grabow, J.-U.; Schnell, M.; Mack, J.; Scott, L. T.; Kuczkowski, R. L. *J. Am. Chem. Soc.* **2005**, *127*, 4345.

(10) (a) Kroto, H. W.; Heath, J. R.; O'Brien, S. C.; Curl, R. F.; Smalley, R. E. *Nature* **1985**, *318*, 162. (b) Zhang, Q. L.; O'Brien, S. C.; Heath, J. R.; Liu, Y.; Curl, R. F.; Kroto, H. W.; Smalley, R. E. *J. Phys. Chem.* **1986**, *90*, 525. (c) Smalley, R. E. *Acc. Chem. Res.* **1992**, *25*, 98.

(11) Pope, C. J.; Marr, J. A.; Howard, J. B. *J. Phys. Chem.* **1993**, *97*, 11001.

(12) (a) Richter, H.; Mazyar, O. A.; Sumathi, R.; Green, W. H.; Howard, J. B.; Bozzelli, J. W. *J. Phys. Chem. A* **2001**, *105*, 1561. (b) Richter, H.; Grieco, W. J.; Howard, J. B. *Combust. Flame* **1999**, *119*, 1.

(13) Harris, S. J.; Weiner, A. M.; Blint, R. J. *Combust. Flame* **1988**, *72*, 91.

(14) (a) Frenklach, M.; Clary, D. W.; Gardiner, W. C.; Stein, S. E. *Proc. Combust. Inst.* **1985**, *20*, 887. (b) Frenklach, M.; Warnatz, J. *Combust. Sci. Technol.* **1987**, *51*, 265. (c) Frenklach, M.; Wang, H. *Proceedings of the 23rd International Symposium on. Combustion*; The Combustion Institute: Pittsburgh, PA, 1990; p 1559. (d) Frenklach, M. *Proceedings of the 26th International Symposium on Combustion*; The Combustion Institute: Pittsburgh, PA, 1996; p 2258.

(15) Wauters, S.; Marin, G. B. *Ind. Eng. Chem. Res.* **2002**, *41*, 2379.

(16) Vereecken, L.; Peeters, J.; Bettinger, H. F.; Kaiser, R. I.; Schleyer, P. v. R.; Schaefer, H. F., III. *J. Am. Chem. Soc.* **2002**, *124*, 2781.

(17) Wauters, S.; Marin, G. B. *Chem. Eng. J.* **2001**, *82*, 267.

(18) Van Speybroeck, V.; Van Neck, D.; Waroquier, M.; Wauters, S.; Saeys, M.; Marin, G. B. *Int. J. Quantum Chem.* **2003**, *91*, 384.

(19) Van Speybroeck, V.; Van Neck, D.; Waroquier, M.; Wauters, S.; Saeys, M.; Marin, G. B. *J. Phys. Chem. A* **2000**, *104*, 10939.

(20) Van Speybroeck, V.; Borremans, Y.; Van Neck, D.; Waroquier, M.; Wauters, S.; Saeys, M.; Marin, G. B. *J. Phys. Chem. A* **2001**, *105*, 7713.

(21) Van Speybroeck, V.; Reyniers, M. F.; Marin, G. B.; Waroquier, M. *Chem. Phys. Chem.* **2002**, *3*, 863.

(22) Van Speybroeck, V.; Hemelsoet, K.; Waroquier, M.; Marin, G. B. *Int. J. Quantum Chem.* **2004**, *96*, 568.

(23) de Bruin, T. J. M.; Lorant, F.; Toulhoat, H.; Goddard, W. A., III. *J. Phys. Chem. A* **2004**, *108*, 10302.

(24) Hemelsoet, K.; Van Speybroeck, V.; Marin, G. B.; De Proft, F.; Geerlings, P.; Waroquier, M. *J. Phys. Chem. A* **2004**, *108*, 7281.

(25) Saeys, M.; Reyniers, M. F.; Marin, G. B.; Van Speybroeck, V.; Waroquier, M. *J. Phys. Chem. A* **2003**, *107*, 9147.

(26) Saeys, M.; Reyniers, M. F.; Van Speybroeck, V.; Waroquier, M.; Marin, G. B. *Chem. Phys. Chem.* **2006**, *7*, 188.

(27) Hemelsoet, K.; Moran, D.; Van Speybroeck, V.; Waroquier, M.; Radom, L. *J. Phys. Chem. A* **2006**, *110*, 8942.

(28) (a) Mebel, A. M.; Lin, M. C.; Yu, T.; Morokuma, K. *J. Phys. Chem. A* **1997**, *101*, 3189. (b) Nicolaides, A.; Smith, D. M.; Jensen, F.; Radom, L. *J. Am. Chem. Soc.* **1997**, *119*, 8083.

(29) Kasai, P. H.; Clark, P. A.; Whipple, E. B. *J. Am. Chem. Soc.* **1970**, *92*, 2640.

(30) Chen, R. H.; Kafafi, S. A.; Stein, S. E. *J. Am. Chem. Soc.* **1989**, *111*, 1418.

(31) Wang, H.; Frenklach, M. *J. Phys. Chem.* **1993**, *97*, 3867.

(32) Aihara, J-I; Fujiwara, K.; Harada, A.; Ichikawa, H.; Fukushima, K.; Hirota, F.; Ishida, T. *J. Mol. Struct. (THEOCHEM)* **1996**, *366*, 219.

(33) Cioslowski, J.; Liu, G.; Martinov, M.; Piskorz, P.; Moncrieff, D. *J. Am. Chem. Soc.* **1996**, *118*, 5261.

(34) Van Speybroeck, V.; Marin, G. B.; Waroquier, M. *Chem. Phys. Chem.* **2006**, accepted.

(35) Frisch, M. J.; Trucks, G. W.; Schlegel, H. B.; Scuseria, G. E.; Robb, M. A.; Cheeseman, J. R.; Montgomery, Jr., J. A.; Vreven, T.; Kudin, K. N.; Burant, J. C.; Millam, J. M.; Iyengar, S. S.; Tomasi, J.; Barone, V.; Mennucci, B.; Cossi, M.; Scalmani, G.; Rega, N.; Petersson, G. A.; Nakatsuji, H.; Hada, M.; Ehara, M.; Toyota, K.; Fukuda, R.; Hasegawa, J.; Ishida, M.; Nakajima, T.; Honda, Y.; Kitao, O.; Nakai, H.; Klene, M.; Li, X.; Knox, J. E.; Hratchian, H. P.; Cross, J. B.; Bakken, V.; Adamo, C.; Jaramillo, J.; Gomperts, R.; Stratmann, R. E.; Yazyev, O.; Austin, A. J.; Cammi, R.; Pomelli, C.; Ochterski, J. W.; Ayala, P. Y.; Morokuma, K.; Voth, G. A.; Salvador, P.; Dannenberg, J. J.; Zakrzewski, V. G.; Dapprich, S.; Daniels, A. D.; Strain, M. C.; Farkas, O.; Malick, D. K.; Rabuck, A. D.; Raghavachari, K.; Foresman, J. B.; Ortiz, J. V.; Cui, Q.; Baboul, A. G.; Clifford, S.; Cioslowski, J.; Stefanov, B. B.; Liu, G.; Liashenko, A.; Piskorz, P.; Komaromi, I.; Martin, R. L.; Fox, D. J.; Keith, T.; Al-Laham, M. A.; Peng, C. Y.; Nanayakkara, A.; Challacombe, M.; Gill, P. M. W.; Johnson, B.; Chen, W.; Wong, M. W.; Gonzalez, C.; Pople, J. A. Gaussian 03, Revision C2; Gaussian, Inc.: Wallingford, CT, 2004.

(36) (a) Becke, A. D. *J. Chem. Phys.* **1993**, *98*, 5648. (b) Stephens, P. J.; Devlin, F. J.; Chabalowski, C. F.; Frisch, M. J. *J. Phys. Chem.* **1994**, *98*, 11623.

(37) Krishnan, R.; Binkley, J. S.; Seeger, R.; Pople, J. A. *J. Chem. Phys.* **1980**, *72*, 650.

(38) Smith, D. M.; Nicolaides, A.; Golding, B. T.; Radom, L. *J. Am. Chem. Soc.* **1998**, *120*, 10223.

(39) Coote, M. L. *J. Phys. Chem. A* **2004**, *108*, 3865.

(40) Scott, A. P.; Radom, L. *J. Phys. Chem.* **1996**, *100*, 16502.

(41) Lynch, B. J.; Truhlar, D. G. *J. Phys. Chem. A* **2001**, *105*, 2936.

(42) Zhao, Y.; Lynch, B. J.; Truhlar, D. G. *Phys. Chem. Chem. Phys.* **2005**, *7*, 43.

(43) Boese, A. D.; Martin, J. M. L. *J. Chem. Phys.* **2004**, *121*, 3405.

(44) (a) Laidler, K. J. *Chemical Kinetics*; HarperCollins Publishers Inc.: New York, 1987. (b) McQuarrie D. A.; Simon, J. D. *Physical Chemistry*−A Molecular Approach; University Science Books: Sausalito, CA, 1997.

(45) Eckart, C. *Phys. Rev.* **1930**, *35*, 1303.

(46) Truong, T. N.; Duncan, W. T.; Tirtowidjojo, M. *Phys. Chem. Chem. Phys.* **1999**, *1*, 1061 and references therein.

(47) Troe, J. *J. Chem. Phys.* **1977**, *66*, 4758.

(48) Heuts, J. P. A.; Gilbert, R. G.; Radom, L. *Macromolecules* **1995**, *28*, 8771.

(49) (a) Vansteenkiste, P.; Van Speybroeck, V.; Marin, G. B.; Waroquier, M. *J. Phys. Chem. A* **2003**, *107*, 3139. (b) Van Speybroeck, V.; Vansteenkiste, P.; Van Neck, D.; Waroquier, M. *Chem. Phys. Lett.* **2005**, *402*, 479.

(50) Van Cauter, K.; Van Speybroeck, V.; Vansteenkiste, P.; Reyniers, M. F.; Waroquier, M. *Chem. Phys. Chem.* **2006**, *7*, 131.

(51) The component absolute energies, ZPVEs and thermal corrections are presented in Table S2 of the Supporting Information.

(52) Cioslowski, J.; Liu, G.; Moncrieff, D. *J. Org. Chem.* **1996**, *61*, 4111.

(53) (a) Bell, R. P. *Proc. R. Soc. London, Ser. A* **1936**, *154*, 414. (b) Evans, M. G.; Polanyi, M. *Trans. Faraday Soc.* **1938**, *34*, 11.